Title:

Quantifying the effectiveness of mountain terraces on soil erosion protection with sediment traps and dry-stone wall laser scans

Author(s):

Camera[1, 2], C., Djuma[1], H., Bruggeman[1], A., Zoumides[1], C., Eliades[1], M., Charalambous[1], K., Abate[3, 4], D., Faka[3], M.

Affiliation(s):

[1] Energy Environment and Water Research Center, The Cyprus Institute

[2] Dipartimento di Scienze della Terra "A. Desio", Università degli Studi di Milano

[3] Science and Technology in Archaeology Research Center, The Cyprus Institute

[4] Centre of Archaeology, Staffordshire University

Corresponding Author:

Corrado Camera
Dipartimento di Scienze della Terra 'A. Desio'
Università degli Studi di Milano
e-mail: corrado.camera@unimi.it
ph: +39 02 50315548 -

Version:

Accepted manuscript version of the paper published in Catena
(https://doi.org/10.1016/j.catena.2018.07.017)

Highlights

- On a terraced vineyard, we measured a soil erosion rate from 2.4 to 3.2 Mg ha^{-1} y^{-1}
- Dry-stone wall degradation increased soil loss by a factor of 3.8
- Erosivity index (EI30) has strong correlation with measured soil loss
- Soil loss is affected by drainage area and degraded dry-stone wall sections in it
- Laser scanner could not furnish reliable information on dry-stone wall degradation

Abstract:

Mountain depopulation in the Mediterranean region over the past decades has led to a decline in the use and maintenance of agricultural terraces and consequently the collapsing of dry-stone walls, which can increase soil erosion rates and downstream sedimentation. A field experiment has been set up on a degrading terraced hillslope in the Troodos Mountains of Cyprus, to quantify the effectiveness of terrace maintenance on protecting cultivated land against soil erosion. The monitored site is cultivated with grapes. The terrace riser (22 m long) that forms the linear outlet of the hillslope has 11.4 m of standing dry-stone wall and 10.6 m of collapsed wall. It has been instrumented with seven 1m wide sediment traps, three on standing sections of the wall and four on collapsed sections. When dry, sediment was collected from the traps after rainfall events, from December 2015 to November 2017. Uncertainties in the drainage areas of the 31.5-m long slope were quantified both for the terrace wall and for the individual traps through hydrologic delineations based on a detailed topographic survey. The sediment data were complemented by laser scanner surveys that were conducted in November 2015, May 2016 and April 2017, on a dry-stone terrace wall upslope from the outlet section. Wall degradation was assessed from the consecutive 3D model reconstructions. Rainfall was 469 mm in the first year and 515 mm in the second year and the average erosivity was 1148 MJ mm ha^{-1} h^{-1} y^{-1}. The average soil erosion rate was 2.4 Mg ha^{-1} y^{-1}, when linear drainage areas are considered (693 m^2), 3.2 Mg ha^{-1} y^{-1} when the borders are delineated with the topographic data (520 m^2). Nearly half of the soil erosion (43%) occurred during two very intense rainfall events (maximum 30-min intensity exceeding 35 mm h^{-1}), out of the 34 monitored events. Erosion from standing terrace sections was 3.8 less than the erosion from the collapsed sections. For the scanned terrace wall, soil erosion from the standing sections was 2.2 lower than from the degraded sections. The laser scanner surveys identified some preferential erosion paths, but failed to recognize single stone collapses, whereas possible wall displacement was masked by scanning artefacts. The sediment traps were found to be an effective method for understanding and quantifying soil erosion in terraced mountain environments, while further research is needed to develop a more rigorous acquisition procedure for laser scanner surveys to derive useful information on wall degradation.

Keywords:

Soil water erosion, Agricultural terrace, Mediterranean vineyard, Monitoring experiment, Sediment traps; Terrestrial laser scanning.

1. Introduction

Dry stone walls have been built around the Mediterranean basin for millennia (Tarolli et al., 2014). In Cyprus, dry stone terraces date back to the Bronze Age (Fall et al., 2012). In general, terraces were created to allow agriculture in mountain environments, and served to reduce the degrading effect of soil erosion by controlling the surface runoff velocity and facilitating water infiltration in the soil. Terraces act as sediment traps storing the washed-off soil material within the hillslope. The sediment that accumulates behind the dry-stone walls creates suitable land for farming. Although their main purpose is food production, terraces have been also recognized as sustainable land management practices for water retention and control of soil erosion in sloping environments (Li et al., 2014). Dry-stone terraces provide an intensive cultivation form, which requires little mechanical aid but high input in terms of labor (Rolé, 2007).

In the steep mountainous areas of Cyprus, erosion by water is a key soil threat (Zoumides et al., 2017). Around the small rural communities in the mountains, large areas have been converted into agricultural terraces, mainly for vineyard cultivations. Similarly, to many other rural areas in the Mediterranean (e.g. see García-Ruiz and Lana-Renault, 2011), the population of the communities in the Troodos Mountains, the main mountain range of the island, has decreased substantially over the past 30 years. As a result, many of the mountain terraces are no longer cultivated and terrace walls are poorly maintained, if at all, causing a progressive degradation of the landscape. In some areas completely abandoned long ago, nature is taking over, thus reducing soil erosion. In such cases, soil erosion is more gradual than on recently abandoned or poorly maintained land, as it has also been observed in other terraced (e.g., Brandolini et al., 2017; Modica et al., 2017) and non-terraced (e.g., Nasta et al., 2017) areas in the Mediterranean Region.

A limited number of studies have tried to quantify soil erosion in terraced environments, either through field research or modelling or both (Dorren and Rey, 2004; Koulouri and Giourga, 2007; Lesschen et al., 2008; Arnaez et al., 2011; Bevan and Conolly, 2011; Nunes et al., 2016; Djuma et al. 2017). The observations and results of these studies are highly contrasting, and a wide range of soil erosion rates have been reported (0.015 – 87 Mg ha^{-1} y^{-1}). The effectiveness of well-maintained terraced hillslopes, as opposed to poorly-maintained terraced hillslopes or natural hillslopes, also varies widely in the literature, subject to different climatalogical conditions (Chow et al., 1999; Dorren and Rey, 2004).

Conversely, due to their socio-economic importance, extensive literature can be found about soil erosion rates in vineyards. Prosdocimi et al. (2016) published a comprehensive review study, in which they create a database of erosion rates in the Mediterranean Region. In doing so, the authors quantitatively summarize the role of different erosion factors, as also investigated by many recent studies (e.g. Biddoccu et al., 2017; Cerdà et al., 2017; Napoli et al., 2017; Rodrigo-Comino et al., 2016; Lieskovsky and Kenderessy, 2014). Although vineyards on terraces are mentioned, no specific analysis of these environments is included, neither as topographical characteristic nor as soil conservation technique. A recent review study by Rodrigo-Comino (2018) focused on soil erosion rates in vineyards around the world. The author derived ranges of soil erosion rates based on the location (country) of study areas and the methodological approach. Also, he suggested to include social and economic aspects in soil erosion studies to help farmers apply effective management strategies. The author did not specifically consider the presence of agricultural terraces or other conservation practices in the reviewed studies, he only mentioned that poorly designed structures can canalize water and increase sediment loss.

In the last decade, ground-based laser and imaging techniques have been increasingly developed and applied in various geoscience domains, due to the growth of computing capabilities, the development of high performance digital sensors and the booming of visual software innovations (Eltner et al., 2016; Westoby et al., 2012). Their application in soil erosion assessments include various studies that compared simple and low-cost Structure from Motion (SfM) techniques with more expensive, high accuracy ground-based LiDAR acquisitions (e.g., Gomez-Gutierrez et al., 2014; Smith and Vericat, 2015). In this regard, Prosdocimi et al. (2015) found SfM methods to be comparable with Terrestrial Laser Scanner (TLS) acquisitions in terms of accuracy, recognition of erosion areas, and calculation of eroded volumes, while analyzing river bank erosion features. Nouwakpo et al. (2016) compared the two techniques on both bare and vegetated soils (up to 77% cover). They found that the two techniques are both reliable and comparable to each other on bare soil, while on vegetated areas the combination of the two techniques leads to the best recognition of changes in the micro-topography. Eltner and Baumgart (2015) looked specifically at the accuracy constraints of TLS methods for multi-temporal surface changes detection. DeLong et al. (2018) applied repeated TLS surveys to monitor post-wildfire soil erosion in the lower 2.7 ha of a catchment (75 ha in total) located in Arizona, USA. The method allowed to recognize and differentiate effects of different erosional processes (overland flow, rill, gully, deposition) by detecting changes in the topography down to 5 mm. Previous studies on post-wildfire erosion (e.g. Staley et al., 2014; Orem and Pelletier, 2015) applied multi-temporal TLS surveys and detected sub-centimeter topographic changes, too. Other studies focused on the reconstruction of 3D models with SfM to determine the evolution of rills and gullies (Di Stefano et al., 2017; Frankl et al., 2015). These authors showed the effectiveness of these methods, which on average led to errors in the calculation of eroded volumes lower than 15% compared to traditional measurement techniques, namely profilometer and measuring tape. Soil erosion processes have been also studied by TLS at the laboratory scale (e.g. Balaguer-Puig et al., 2017). Preti et al. (2013) performed TLS scans to obtain a front-viewed 3D digital model of a dry-stone retaining wall. The resulting model had a resolution of 0.01 m, allowing recognition of single wall stones, and was optimal for stress-strain stability simulations. In addition, Preti et al. (2013) and Tarolli et al. (2015) used TLS surveys to derive high resolution Digital Terrain Models (DTMs) to perform a hydro-geomorphological analysis of terraced vineyards. They used the DTMs to recognize preferential accumulation flow paths caused by terraces and applied the Relative Path Impact Index (RPII) proposed by Tarolli et al. (2013). However, no comprehensive study can be found in the literature that combines sediment loss measurements by traps or troughs, with multi-temporal TLS surveys to quantify erosion from hillslopes with degrading dry-stone walls.

The overarching goal of this study is to quantify the effectiveness of maintaining and restoring terraces retained by dry-stone walls for reducing soil erosion by water. Specifically, a monitoring experiment was set up: i) to compare erosion rates from non-degraded (standing) and degraded (fully or partly collapsed) dry-stone wall sections and to quantify the amount of soil eroded in a typical terraced vineyard, ii) to analyze relations between erosion from terraces, rainfall, erosivity and runoff; iii) to complement traditional soil erosion measurements (soil traps) with dry stone wall degradation observations derived from terrestrial laser scans.

2. Case study area and monitoring site

Mountain agriculture in the Troodos Mountains of Cyprus consists mainly of small, poorly maintained, terraced plots cultivated for family use. According to the declared 2016 agricultural plots, as registered in the Cyprus Agricultural Payments Organization (CAPO) database, grape, fruit trees and nuts are the main crops at elevations above 800 m a.s.l. These crops occupy 690 ha, 676 ha and 16 ha, respectively, out of a total declared agricultural area of 1817 ha. The average plot size is 0.16 ha for grapes, 0.11 ha for fruit trees, and 0.08 ha for nut trees. The average slope of the Troodos region above 800 m a.s.l. is 42%.

The monitoring site is located in the upstream part of the 112-km^2 Peristerona Watershed, on the northern slope of the Troodos Mountains. A map showing the location of the case study area and monitoring site is presented in Fig. 1. The upstream area ranges from 900 to 1,540 m a.s.l. and has a mean slope above 40%. Intrusive rocks (gabbro, diabase and basal group) of the Troodos ophiolitic sequence dominate its geology. The main land cover comprises of sclerophylous vegetation and mountain agriculture on dry-stone terraces. The average annual precipitation is around 750 mm (1980-2010), with daily extremes that can reach up to 170 mm (Camera et al., 2014a). Temperature ranges from an average daily minimum temperature of 3 ºC in January and February to an average daily maximum temperature of 31 ºC in July and August. In general, the Troodos Mountains are characterized by a warm temperate climate, with most rainfall occurring during the winter months, which is typical for the Mediterranean region (Zittis et al., 2017).

The monitoring site is a hillslope cultivated with grapes, located in the mountain community of Alona, at an elevation of 1,300 m a.s.l. Land use, maintenance conditions, and slope angle (50%) are representative of the terraced agricultural plots in the Troodos Mountains. Soil texture is gravelly sandy loam, as analyzed on replicate samples from 0-15 and 15-30-cm depths, using the international standard BS ISO 11277 (2009). Soil organic carbon (SOC) on the terraces is 3.1% at 0-15 cm and 2.8% at 15-30 cm depth. These values were obtained from eight samples per depth, with the loss-on-ignition method, as recommended by Hoogsteen et al. (2015). Four bulk density samples were collected at the top soil layer (0-15 cm depth) with 100-cm^3 rings and the dry bulk density was computed after drying and weighting. The average value of the four samples was 1.6 g cm^{-3}. Soil depth was measured with a 1 -m long utility probe hammered in the soil at 15 locations along the lowest terrace bench and was found to vary from 0.3 m (upslope, far from the wall) to more than 1.0 m (downslope, next to the wall).

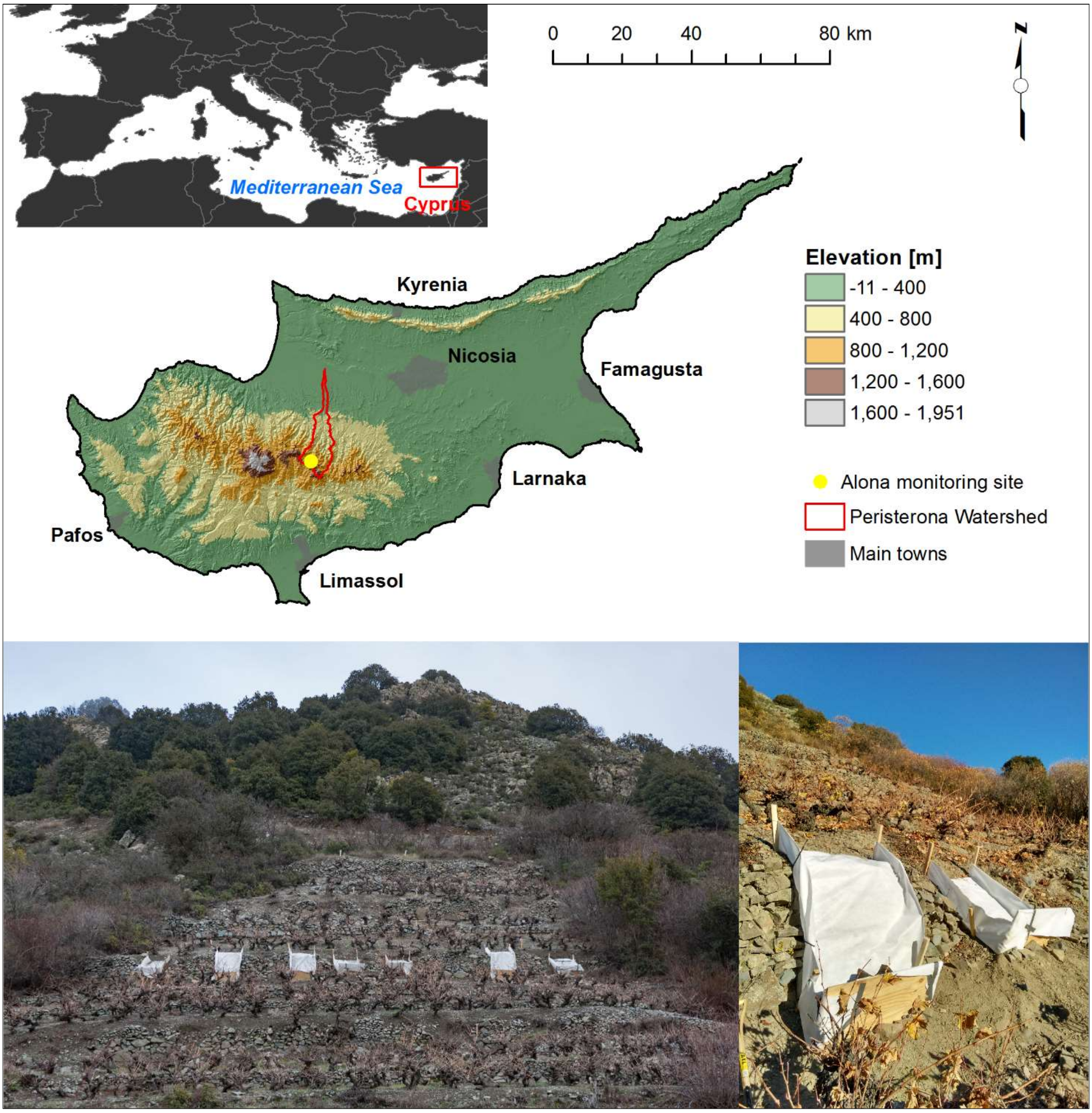

Fig. 1: Location of the Peristerona Watershed case study area and the Alona monitoring site. The images show the sediment traps used for capturing and measuring the eroded soil.

The monitoring hillslope is delimited downslope by a terrace with a 1.25 m high dry-stone wall, and a 22 m long and 8 m wide bench. The terrace is poorly maintained, and the dry-stone wall presents both standing and degraded (fully or partly collapsed) sections. The upslope area includes four terraces with similar maintenance status and a strip of natural vegetation. A dirt road is located at the top of the hillslope. The dirt road is bordered by a small dike on its lower edge, preventing runoff from upslope areas to enter the terraced field. The average length of the hillslope between the edge of the road and the most downslope dry-stone wall is 31.5 m.

3 Materials and Methods

3.1 Experimental design and field data collection

Considering the complexity of this human-modified mountain environment, no hillslopes can be found with comparable physical and geometric characteristics (e.g., slope angle, elevation, area, number of terraces in the area) for monitoring effectiveness of maintaining terraces. Therefore, erosion was monitored from standing (treatment) and degraded (no treatment) sections of dry-stone wall on a single hillslope. Seven sediment traps were installed at the most downslope terrace of the monitored hillslope, on 24 November 2015 (see Fig. 2). The 22 m long terrace has three sections of standing dry-stone wall (11.4 m total) and four sections of collapsed wall (10.6 m total). The 1 m wide traps were placed in the middle of each collapsed and standing wall section.

An automatic, tipping bucket (0.2 mm) rain gauge (Davis Rain Collector Vantage Pro2) was installed on the monitoring hillslope. Rainfall was also recorded with a manual rain gauge (ClimeMET CM1016), with a 0.1-m diameter funnel. Fifteen soil moisture sensors were placed in the soil of the trap-equipped terrace, at six randomly selected locations within a radius of 10 m from the meteorological station (see Fig 2). Sensors were installed at 10, 30 and 50 cm depths in three locations with medium soil depth (~ 60 cm), and at 10 and 30 cm depths in three locations with shallow soil depth (~40 cm).

Three consecutive laser scanner surveys were made from the facade of the dry-stone wall located upslope of the trap-equipped terrace (see Fig. 2). Due to the presence of thick natural vegetation on the sides of the targeted terrace, the surveys covered 17.1 m out of the 21.8 m of the terrace wall.

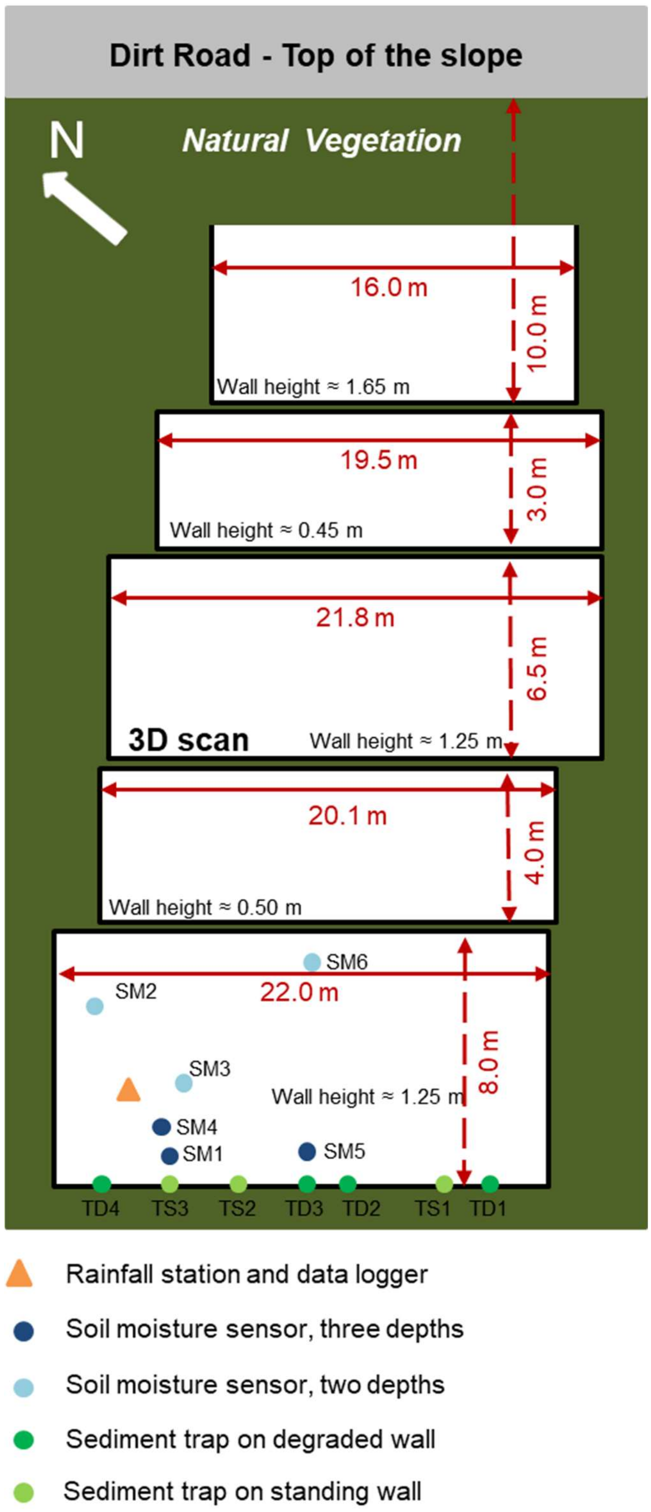

Fig. 2: Scheme of the monitoring experiment; rectangles represent single terrace benches, 3D scan indicates the location of the terrestrial laser scanner dry-stone wall facade survey.

3.1.1 Soil erosion assessment with sediment traps

Each sediment trap is constructed with a geotextile nailed to the soil at the top and confined by wooden sticks and boards on the sides and at the bottom, to catch the sediment-laden surface runoff from the terrace bench (see Fig. 1). The non-woven geotextile has a weight of 200 g/m^2 and an opening size of 0.06 mm (O90, i.e. 90% of the passing material has a diameter equal to or less than 0.06 mm). The accumulated sediment was collected from the traps after rainfall, between December 2015 and November 2017. Sediment was collected when the traps were dry, as a substantial amount of fine soil particles remained stuck to the geotextile of the traps when they were wet. Consequently, most collection intervals included multiple rainfall events. Sediment was collected for a total of 34 events.

3.1.2 Sediment trap drainage areas

Sediment trap drainage areas were calculated based on slope length, assuming a linear slope as in many erosion models (e.g., PESERA - Kirkby et al., 2008). The linear slope length represents the most immediate approximation of surface runoff flow paths and can be easily applied. Secondly, trap drainage areas were derived, based on a detailed topographic survey, to account for and discuss uncertainties related to the estimate of soil erosion rates. To define topography-based drainage areas, the coordinates and elevation of 1387 points were acquired through a differentially-corrected Global Navigation Satellite System (GNSS) survey, using a Leica Viva GNSS GS10/GS15. The GNSS was used rather than the laser scanner, as it allowed to obtain ground points without a post-processing filtering, especially in areas with natural vegetation. These observations have an approximate horizontal accuracy of 0.005 m and a vertical accuracy of 0.010 m. The data point acquisition was performed during three non-consecutive days in April 2016. Special attention was given to delineate the standing and degraded sections of the terrace walls. The data were collected in the World Geodetic System 84 (WGS84) using the projection of the Universal Transverse Mercator, zone 36N (UTM36N).

3.1.3 Relations between soil erosion rates, rainfall erosivity and intensity

Precipitation was recorded by the installed rain gauge every 5 minutes. The soil moisture sensors measured both dielectric permittivity and soil temperature (Decagon 5TM). The instruments were connected to a datalogger (OTT netDL-500) for continuous data acquisition. The manual rain gauge was installed in December 2015. The automatic rain gauge and 12 out of 15 soil moisture sensors were installed in April 2016; monitoring started in May after testing. The three soil moisture sensors at location 6 started acquiring data only on the 25 October 2016, because of problems with the datalogger settings. Dielectric permittivity and soil temperature, as measured by the 15 installed soil moisture sensors, were recorded every hour. The datalogger sent the data, through GPRS connection, to a remote server located at The Cyprus Institute in Nicosia every four hours. Soil moisture was computed from the dielectric permittivity with the Topp equation (Topp et al., 1980). Between November 2015 and April 2016, rainfall data (10 minutes interval) were obtained from the Cyprus Meteorological Service (CMS) station in Polystipos (around 2 km away from the monitoring site). During that time, rain was also recorded with the manual rain gauge on at the research site.

3.1.4 Laser scanner surveys

Laser scanner surveys were performed on 25 November 2015 (after the installation of the sediment traps), 16 May 2016, and 3 April 2017 (at the end of the wet season). Scans were made on the facade of the dry-stone wall, indicated in Fig. 2, with the primary aim to evaluate structural changes (e.g., wall displacements, fall of single stones, soil back cuts). The surveys covered 17.1 m out of the 21.8 m of the dry-stone wall under analysis. The drainage area of the scanned terrace wall measures 333 m^2, assuming a linear slope. To ensure that the three surveys were comparable, a topographical network was established. Ground control points were installed to cover the whole study area and their position was georeferenced with a Total Station (Leica Viva TS11) and GNSS System (Leica Viva GNSS GS10/GS15). Scans were performed using a phase shift laser scanner (Surphaser® 25HSX, IR_X configuration), which includes an optical working range between 0.4 and 30 m, a noise range of 0.1 mm at 3 m, and an uncertainty range lower than 0.5 mm at 5 m. In November 2015, the scanner was placed in four positions, yielding an average scanner-to-object distance of 3.5 m, which allowed an X–Y resolution of 1.75 mm for each point cloud (equivalent to 35 lines per degree - LPD). In May 2016 and April 2017, the scanner was placed in six positions, keeping an average scanner to object distance of 3.5 m, which allowed an X–Y resolution of 2.45 mm for each point cloud (equivalent to 25 LPD). The higher number of scanning positions in May 2016 and April 2017, in comparison to November 2015, was deemed necessary due to the presence of vine leaves that obstructed the lines of view of the scanner, especially in May 2016. The acquired point clouds included approximately 55 million points for the scans of November 2015 and May 2016, and 50 million points for the scan of April 2017.

3.2 Laboratory analyses

3.2.1 Soil erosion assessment with sediment traps

The sediment collected in the traps was dried in the oven at 110±5 ºC for 12-16 hours (USDA, 2014) and then weighted. The > 2 mm and < 2 mm fractions were isolated by sieving and weighted separately. The measured weight of the sediment (S_{mes}) was adjusted to include the soil lost through the pores of the geotextile (size: P_{090}), as follows:

$$S = \frac{S_{mes}}{1 - X/90} \quad (1)$$

where S is the total soil loss [g], X is the percentage of soil with a diameter equal or less than 0.06 mm [g/g]. The X value was 26%, measured by grain size analysis of soil samples collected in the top layer (0-15 cm), i.e. the soil layer that seems primarily affected by erosion processes, according to site observations. The particle size of the eroded sediment could be influenced by the selectiveness of transport, which could increase the relative amount of fine particles in eroded soil in comparison to coarse particles. However, particles getting trapped in the openings of the geotextile could reduce the loss of fine particles through the geotextile. Both processes are difficult to quantify, but considering their opposite effect, the application of the correction was assumed reasonable.

3.3 Data analyses

3.3.1 Soil erosion assessment with sediment traps

Average soil loss values per event were calculated for degraded and standing sections of dry-stone wall from the seven traps. Assuming a linear slope length of 31.5 m, the soil loss (in Mg ha^{-1}) along the terrace wall (SL_{tot}) was calculated as:

$$SL_{tot} = \sum SL_{dt} \frac{A_{dw}}{A_{dt}} + \sum SL_{st} \frac{A_{sw}}{A_{st}} \quad (2)$$

where SL_{dt} and SL_{st} are the average soil losses [Mg ha^{-1}] collected from traps on degraded and standing wall sections; A_{dt} and A_{st} are the drainage areas [ha] of degraded and standing terrace wall sections covered by traps; and A_{dw} and A_{sw} are the total drainage areas [ha] of degraded and standing wall sections, respectively. Drainage areas were always calculated based on slope length (31.5 m).

To statistically verify the effectiveness of well-maintained versus poorly-maintained terraces in reducing soil erosion, a repeated measures ANOVA (Mangiafico 2016) was performed in R (www.r-project.org) on the soil loss amounts observed in the seven traps [Mg ha^{-1}], with the 34 collection events as the repetition.

3.3.2 Drainage areas

Linear slope areas were calculated by multiplication of the terrace length (or trap width) with the linear slope length (31.5 m) perpendicular to the terrace length. For the topography-based drainage areas from the acquired ground points, a Triangular Irregular Network (TIN) was derived and then transformed in a raster grid with a horizontal resolution of 0.25 m. From the obtained Digital Elevation Model (DEM), the dry-stone wall catchment and single trap drainage areas were defined using the Spatial Analyst in the Hydrology toolbox of ArcGIS® (Version 10.2.1). For the whole hillslope, the most downslope terrace (22 m long) was considered as a linear outlet and its drainage area was calculated accordingly. For traps, considering possible errors in the acquisition and slight changes in the topography following rainfall events or agricultural activities, the drainage areas were calculated both for their precise 1 m location as outlet (called minimum area) and for a 1.5 m outlet, including an extra raster cell on each side of the trap (called maximum area), resulting in a min-max drainage area range for each trap. It was assumed that the whole hillslope minimum and maximum drainage areas coincided; the catchment calculated on a 22.5-m outlet (instead of 22 m) differed less than 5 m^2.

The computed linear slope, minimum and maximum drainage areas were used to quantify the uncertainty of the soil erosion rates over the drainage area of each trap and over the whole hillslope, using Equation 2. Also, to connect the sediment collected in the traps with the hydrologic characteristics of their upslope areas, the lengths of the degraded and standing terrace wall sections within their drainage area were computed.

3.3.3 Relations between soil erosion rates, rainfall erosivity and intensity

The rainfall erosivity (EI30) was calculated for each rainfall event according to the standard RUSLE2 methods (USDA-Agricultural Research Service, 2013). RUSLE2 gives a slightly higher, but overall comparable, erosivity value compared to the original RUSLE equation (Renard et al., 1997), as explained by Nearing et al. (2017). Rainfall events were separated by a minimum 6-hour dry period. For each rainfall event, maximum precipitation intensities for 10 and 60 minutes duration (PMX10 and PMX60) were also calculated. Both the total erosivity (sum of EI30 for all rainfall events) and the maximum EI30 for each sediment collection interval were computed. The runoff ratio erosivity index (Q_REI30) was computed, as suggested by Kinnel (2014), by subtracting the average change in soil moisture from the total rainfall amount of the maximum EI30 event. The average change in soil moisture for each rainfall event was computed from the six soil moisture profiles. Relations between the collected sediment, the erosivities and the maximum rainfall intensities were analyzed.

3.3.4 Laser scanner surveys

Following data acquisition, the point clouds were aligned using the JRC 3D Reconstructor software (Gexcel, 2017). Operations on the point clouds were performed with CloudCompare V2.9 (http://www.danielgm.net/cc/). Four steps were followed: i) manual segmentation of the point clouds to remove vine trees and bushes (all point clouds were segmented together since they were aligned in the same reference system); ii) automatic noise filtering and sampling of the point clouds (separately for each season), to obtain a uniform point to point distance (0.0007 m) for the three models; iii) automatic computation of the distance between the point clouds of different seasons (November 2015 – May 2016, May 2016 – April 2017) on a 0.004 m horizontal resolution grid, and iv) visual splitting of the model to separate standing and degraded wall sections. Cloud-to-cloud distances were then visually analyzed to identify wall degradation processes, i.e., displacements, falling of single stones, main erosion patterns. The filtered distances were converted to volumetric differences by multiplication with pixel areas. Negative and positive volumetric differences were calculated separately to highlight both sediment loss and deposition. The volumetric values were multiplied with soil bulk density to obtain soil weights. Using ArcGIS® (Version 10.2.1), the accuracy of the instrument was summed and subtracted from the calculated cloud-to-cloud distance values to account for measurement uncertainties. This allowed to derive ranges of soil erosion rates after conversion of distances into volumes and weights.

4 Results

4.1 Treatment effectiveness on soil erosion reduction

4.1.1 Soil erosion assessment with sediment traps

Table 1 presents the rainfall, erosivity and soil loss of the two monitoring years (December 2015 – November 2017). The total soil loss of the 693 m^2 linear slope during the study period is 4.8 Mg ha^{-1}, whereas soil with grain size lower than 2 mm amounts to 3.0 Mg ha^{-1}. Rainfall and sediment loss of the two years were comparable, even though the total EI30 was more than double in the first monitoring year. Soil loss from the monitored standing sections was estimated to amount to 0.19 Mg ha^{-1}, while soil loss from degraded wall sections reached 0.78 Mg ha^{-1}. The soil loss ratio between degraded and standing walls is 3.8, indicating a soil loss reduction of 73% by the standing walls. The soil loss of the standing and the degraded wall sections was significantly different ($p \leq 0.01$), according to the repeated measures ANOVA.

Fig. 3 shows the average amount of sediment collected in traps on the degraded and standing wall sections per event (34 in total), together with the estimated total soil loss per hectare for the entire hillslope (22x31.5 m^2), and the precipitation in the intervals between sediment collections. Two erosion events stand out for the large amount of sediment loss, i.e., 4 November 2016 and 10 May 2017. Together, they account for the 43% of the total soil loss over the two monitoring years. Both events had high rainfall intensities (more than 35 mm h^{-1} in 30 minutes and around 20 mm h^{-1} in 60 minutes, see Section 4.1.3). High total rainfall (244.2 mm) was observed for the collection event of 23 January 2017. However, snow and many small rainfall events occurred during the collection interval and soil loss over the whole slope was 0.2 Mg ha^{-1}.

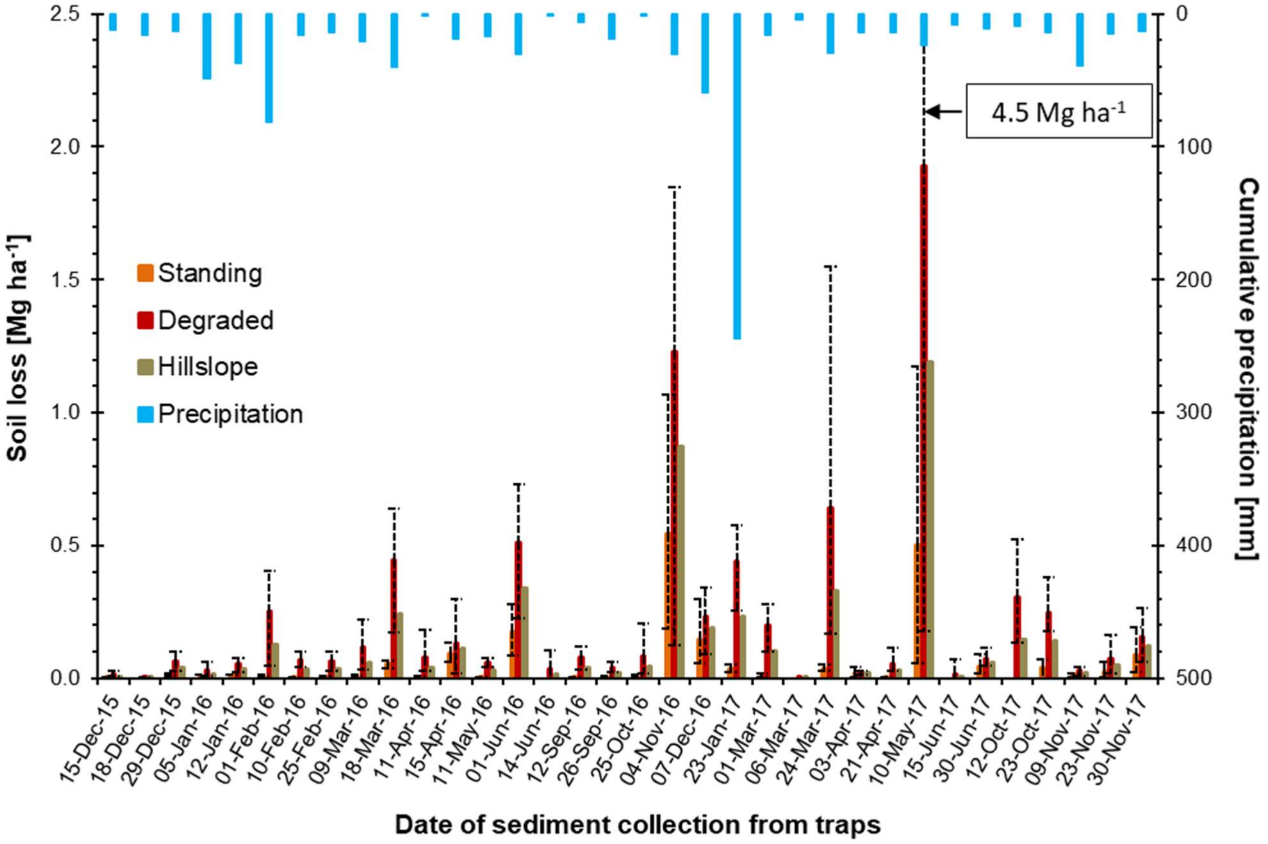

Fig. 3: Total precipitation, average soil loss for degraded and standing wall sections, and for the full hillslope, collected by sediment traps, assuming linear drainage areas, for all collection events. Error bars represent the maximum and minimum soil loss of the four degraded and of the three standing sections.

Table 1: Soil erosion rate, rainfall and erosivity (EI30) for December 2015 – November 2016 and December 2016 – November 2017, calculated assuming linear drainage areas.

Year	Rain [mm]	EI30 [MJ mm ha^{-1} h^{-1} y^{-1}]	Soil erosion rate [Mg ha^{-1} y^{-1}]		
			Degraded	Standing	Hillslope
2016	469.3	1762	3.4	0.9	2.1
2017	514.6	851	4.4	1.0	2.7

4.1.2 Soil erosion range derived from drainage areas

From the topographic survey, the drainage area of the monitored hillslope was found to be 520 m^2, as compared to 693 m^2 for the assumption of a linear slope. Thus, the average soil erosion rate over the hillslope during the two monitoring years could have been as high as 3.2 Mg ha^{-1} y^{-1} (33% higher than that calculated with the reference linear slope).

The location and drainage areas of the sediment traps, as calculated from the detailed topographic survey, are presented in Fig. 4a and Table 2, together with the distribution of the standing and degraded wall sections upslope. Fig. 4b shows the flow accumulation map of the study area, which helps to understand the differences between minimum and maximum drainage areas; in TD4 for example, the large difference between the two drainage areas is due to a flow accumulation line passing through the cell next to the trap. The difference is minor between the drainage area range for traps on standing (2.6 – 73.6 m^2) and degraded (2.3 – 70.0 m^2) wall sections. Averages are similar for the minimum drainage areas, i.e., 39.2 m^2 and 38.9 m^2, for traps installed on degraded and standing wall sections, respectively. A small difference is noticed for the maximum drainage areas, i.e. 62.4 m^2 and 47.5 m^2, for traps installed on degraded and standing wall sections, respectively. The occurrence of degraded and standing sections with similar drainage areas (e.g., TD2 and TS1, TD3 and TS3) indicate that dry-stone wall failure cannot be related to hydrologic processes alone. Possibly, during intense events, obstructions finer than the raster cells (e.g. stones) and features not included in the topography (e.g. vines) could have changed the flow paths of surface runoff, causing runoff concentration and destruction of specific dry-stone wall sections.

To further explore the effect of surface processes on soil erosion at degraded and standing wall sections, Table 2 links the traps with the degraded and standing wall sections located at the terraces upslope, based on their drainage areas. It presents ratios of degraded wall sections, against the complete length of the wall that falls within the maximum drainage areas of the traps. All traps on degraded sections, with the exception of TD1, show higher soil erosion rates for maximum drainage areas than traps on standing sections. This could be affected by the condition of the upslope terraced area where three out of the four traps on degraded sections (TD1, TD2, TD3) also have three degraded walls sections in their uphill drainage areas. Conversely, the traps located on standing sections have only two degraded sections in their upslope drainage areas. For TD2 and TD3, the three degraded upslope wall sections are consecutive, and the standing section is at Wall 2, i.e., the closest to the monitoring terrace. TD1 presents two flow accumulation paths draining in it (Fig. 4b), one of which has an accumulation path that intercepts consecutively degraded sections at Walls 2 and 3, just uphill of the monitored terrace. Despite the very low erosion rate recorded at TD1, this was the most degraded section as observed visually in the field. However, the irregularity of the degraded surface affected the connection between the soil surface and the geotextile, resulting in a lower trap efficiency. A proof of this weak connection and low efficiency could be the ratio between the weights of the material with diameter larger than 2 mm and the total collected sediment; TD1 shows the highest value among all traps. TS1 is the trap showing the lowest soil erosion rate and it is the only trap where the flow accumulation path intersects a degraded section along Wall 2. However, at Walls 3 and 4 it intersects with standing sections.

These evidences show that the soil erosion rates computed from traps increase with the number of flow accumulation paths ending in them and with the interception of consecutive upslope sections of degraded walls. Also, data shows that standing wall sections can effectively reduce erosion rates (e.g. Walls 3 and 4 for TS1, Wall 2 for TD2 and TD3 in comparison to TD1), but may not completely protected the downslope terraces if the upslope flow accumulations paths are long and uninterrupted (e.g. Wall 2 for TD2 and TD3).

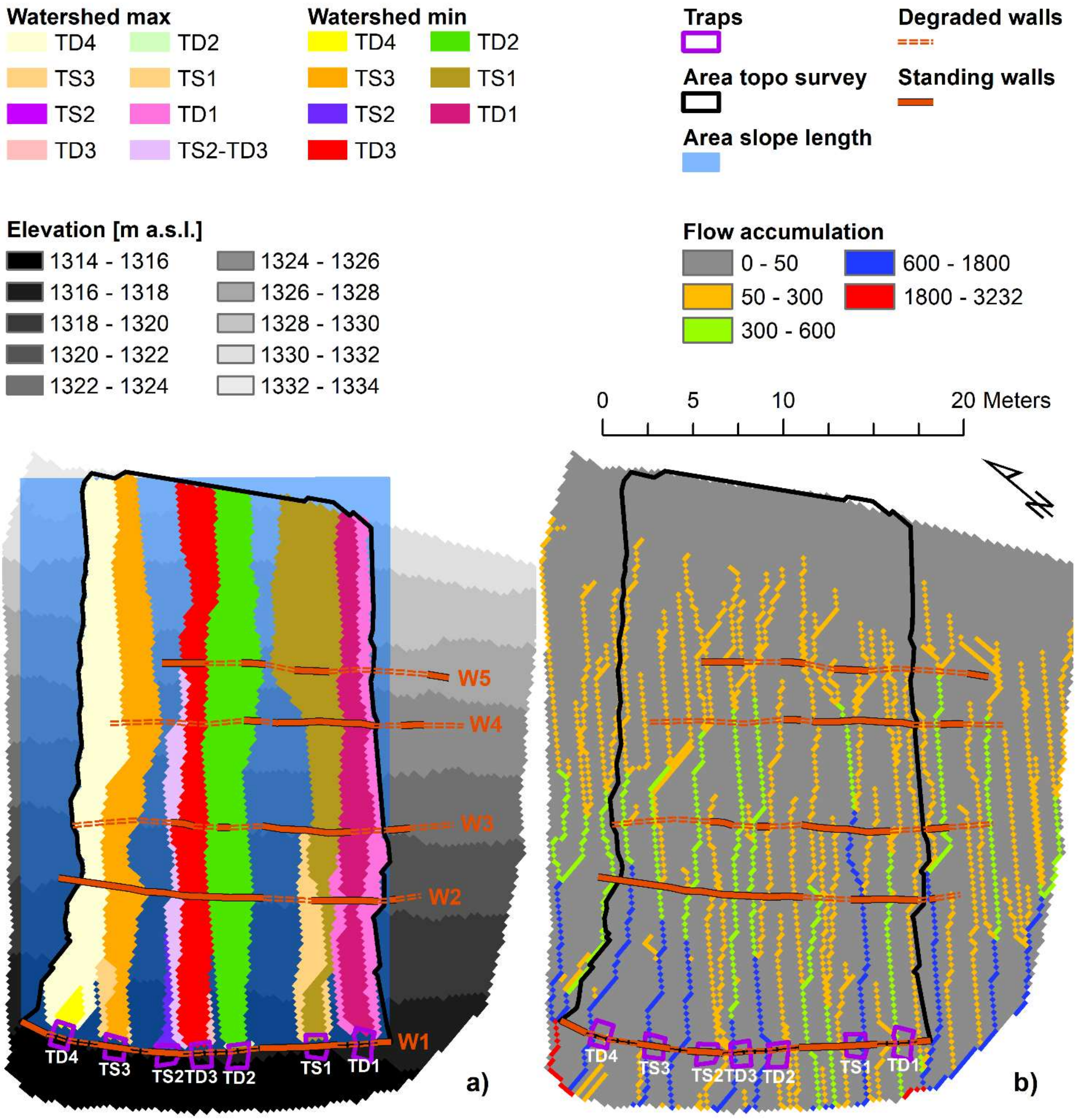

Fig. 4: a) Location and drainage areas (minimum and maximum) of the sediment traps, derived from the detailed topographic survey together with the location of traps and standing and degraded wall sections of the upslope walls (W1 to W5). Drainage areas are plotted on the elevation map. b) The flow accumulation map. TD and TS denote the traps on degraded and standing dry-stone wall sections, respectively.

Table 2: Erosion rate at degraded (TD) and standing (TS) traps for the delineated drainage areas, during the two-year monitoring period, and the ratios of upslope degraded wall length over total wall length inside the maximum drainage area of each trap (from W2 to W5, see Fig. 3). Erosion rate max is calculated with Drainage area min, while Erosion rate min is calculated with Drainage area max.

Trap	Drainage area max [m^2]	Drainage area min [m^2]	Erosion rate min [Mg ha^{-1} y^{-1}]	Erosion rate max [Mg ha^{-1} y^{-1}]	W2 (D) [-]	W3 (D) [-]	W4 (D) [-]	W5 (D) [-]
TD1	59.6	36.6	1.2	1.9	0.07	0.74	0.00	1.00
TD2	70.0	69.9	2.9	2.9	0.00	0.65	0.78	0.62
TD3	60.6	48.2	1.7	2.2	0.00	0.43	1.00	0.16
TD4	59.4	2.3	1.9	49.8	0.00	1.00	1.00	Nat*
TS1	73.6	62.8	0.2	0.2	0.41	0.00	0.00	0.49
TS2	14.3	2.6	1.5	8.0	0.00	0.50	1.00	NW*
TS3	54.4	51.4	1.0	1.1	0.00	1.00	1.00	Nat*

* Nat denotes natural vegetation, and NW means no wall.

4.1.3 Relations between soil loss, rainfall erosivity and intensity

The linear relation between the soil erosion and the EI30 for the hillslope of the 34 collection events was slightly higher when regressing against the maximum event EI30 of the collection intervals (R^2 0.41) than when regressing against the sum of the event EI30 of the collection interval (R^2 0.37). This indicates that most of the sediment was generated by the more erosive rainfall event that occurred between two collection intervals. This can also explain why soil loss in the two monitoring years is comparable, while total erosivity is rather different. Thus, the analysis of the relation between soil loss, rainfall erosivity, maximum rainfall intensities and the runoff ratio erosivity was made for the internal event maxima (see Fig. 5). Figure 5 shows the relations for the 22 events for which the on-site rain gauge as well as the soil moisture data for the runoff computations were available. The best correlation is obtained with EI30, which explained 65% of the variability of the soil loss. The correlation was higher for the EI30 than for Q_REI30. However, the analysis of the runoff from the six soil moisture profiles could only be considered indicative. The computations found zero runoff for six of the twenty-two erosion events.

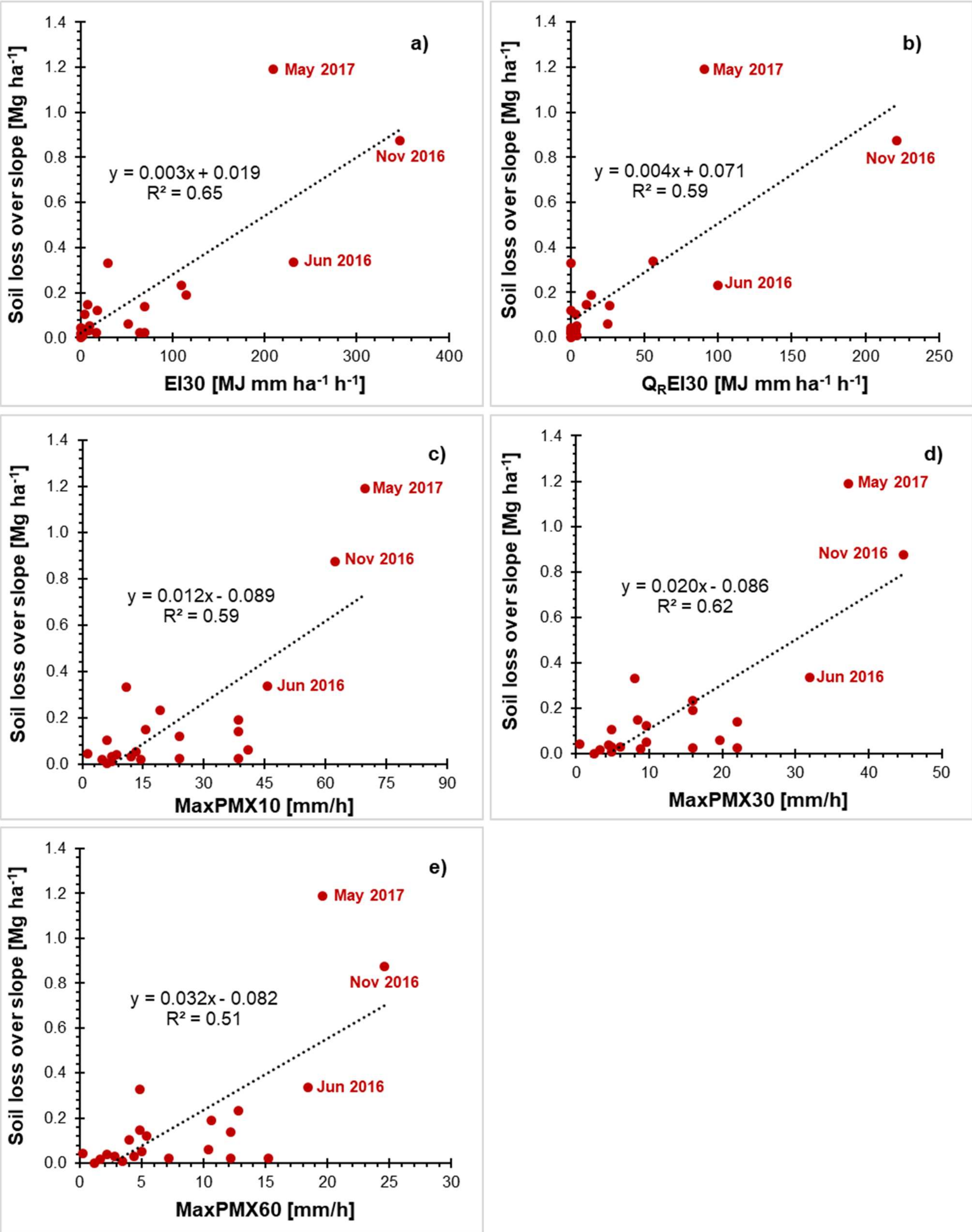

Fig. 5: Correlation between soil loss over the hillslope per unit of drainage area, for 22 sediment collection events, and the maximum rainfall erosivity – EI30 (a), runoff ratio erosivity index – Q_REI30 (b), and the 10-min (c), 30-min (d) and 60-min (e) maximum rainfall intensities of the event – MaxPMX10, MaxPMX30 and MaxPMX60, respectively.

The three events with the largest rainfall intensities and erosivities (Fig. 5) show very different soil losses, thus affecting the correlation analyses. These events occurred in June 2016 (below the regression line), in November 2016 (on the regression line) and in May 2017 (above the regression line). A fourth comparable event occurred in February 2016 and was not part of the 22 events in Fig. 5; this event would have been below the regression line possibly reducing the correlation coefficient.

In Fig. 6, sediment loss and maximum erosivity per event (EI30) are plotted together with hourly average soil moisture at the three depths (10, 30, 50 cm) and the hourly precipitation. Fig. 6 shows that in general, when soil moisture is higher (e.g., after December 2016 in comparison to the previous period), soil loss is also higher for similar rainfall events and erosivities. The May 2017 event was characterized by the highest soil loss, higher soil moisture but lower maximum erosivity than the June and November 2016 events. This indicates that for the soil with higher moisture, saturation runoff might be added to infiltration-excess runoff and result in higher sediment loss. Also, almost no change in soil moisture is observed at 50-cm depth for the two high-intensity events of November 2016 and May 2017. Soil moisture at 50-cm depth is mainly influenced by prolonged periods of moderate water input (rainfall or snowmelt). This means that sediment loss is mainly related to the soil moisture dynamics of the upper soil layer (0-40 cm) only.

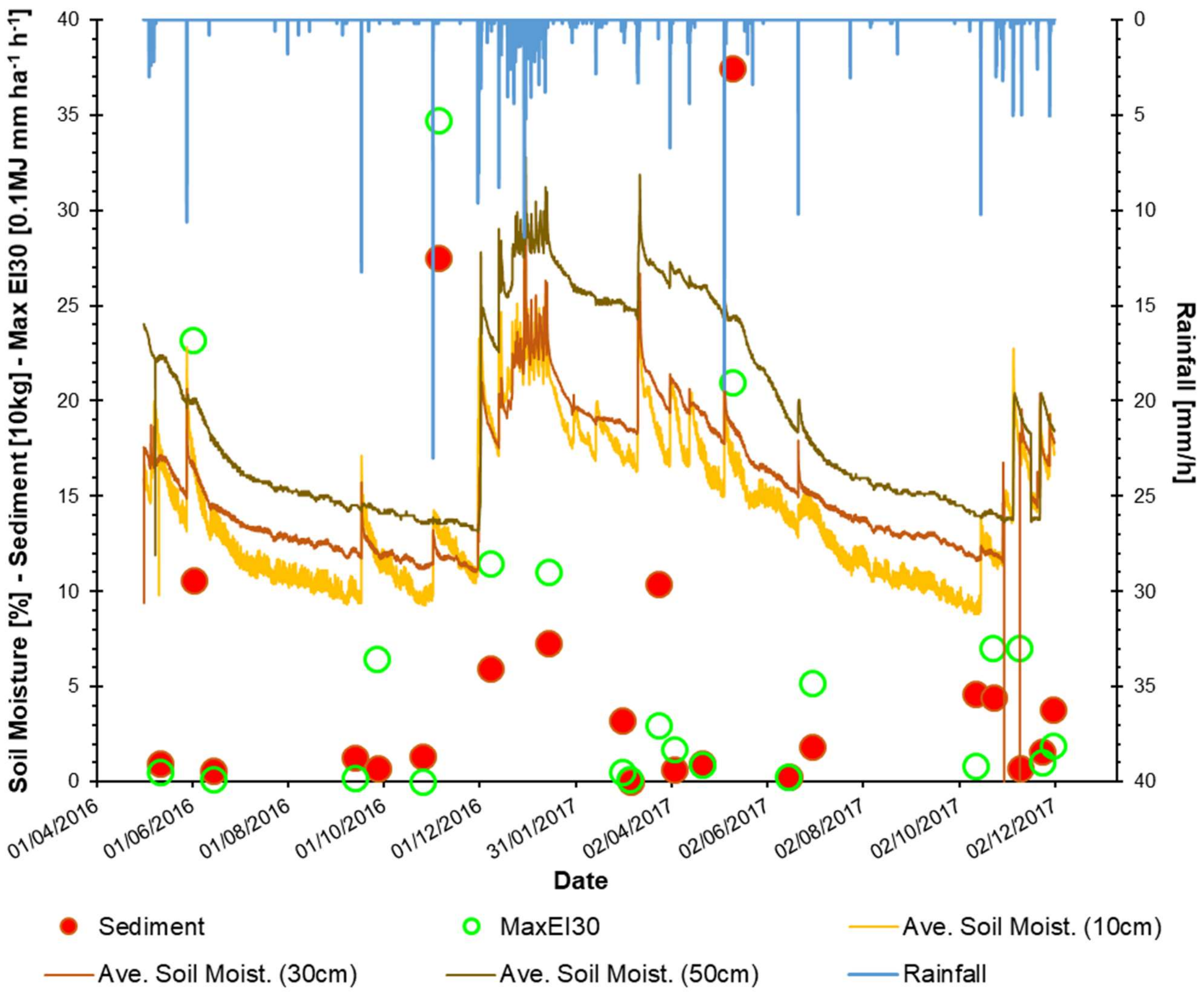

Fig. 6: Average hourly soil moisture (Ave. Soil Moist.) at 10-, 30- and 50-cm depth, hourly rainfall and sediment and maximum erosivity (MaxEI30) for sediment collection events.

4.1.4 Laser scanner survey results

The post-processed outcomes of the laser scanner surveys are presented in Fig. 7 and in Table 3. For each dry-stone wall section, a value of mobilized sediment over the two different time periods is reported. Fig. 7 shows the cloud-to-cloud distances between 3D models of the facade of the wall, as obtained from surveys at different times. Fig. 8 presents photographs of selected degraded and standing sections on the scanned terrace. The two figures highlight three major aspects. First, the only stone collapse (rolling downslope) that was clearly recognized by the method occurred in the second period (May 2016 – April 2017) (Fig. 7). This is indicated by the loss area (< -10 cm) on the top right corner of standing section 6 (SS6), and a similar gain dimension (> 10 cm) at the bottom of the wall. In the same figure, the partially or fully standing dry-stone wall areas often show losses or gains in linear or circular patterns around the stones. These patterns are highlighted by the finely graded dots inside the wall polygons and are attributed to the different laser scanner positioning between the three surveys. The laser beam can enter the voids between stones but, according to the angle, it hits the stones at different depths from the planar surface of the wall, resulting in the observed differences. Inevitably, possible displacements and collapses of stones are not adequately captured. Therefore, despite its high accuracy, the laser scanner method, as applied in this study, generally failed to deliver the expected information on surface changes over standing dry-stone wall areas. For these reasons, these areas were excluded from the computation of soil losses and gains presented in Table 3. Second, in Fig. 7 and for the period Nov 2015 - May 2016, distance values larger than 10 cm on top of the SS6 wall represent grown vegetation. Large distance values are also visible at the far-right section of SS8. In the following season, the distances are again larger than 10 cm meaning that vegetation (e.g. vines, branches, foliage) was not ideally removed from the point cloud of May 2016 while performing the manual segmentation of the three scans together. However, considering only points with cloud-to-cloud distances larger than 10 cm, it was estimated that the introduced error is limited (± 3 kg). Third, at the top of degraded section 7 (SD7, both seasons) the loss areas represent the scarp of the dry-stone wall collapse that is eroding back. A similar behavior can be observed for SD1 and on the left side of SD3 in the May 2016 - Apr 2017 image. This seems the major process responsible for soil loss at this terrace and probably in general in the study area.

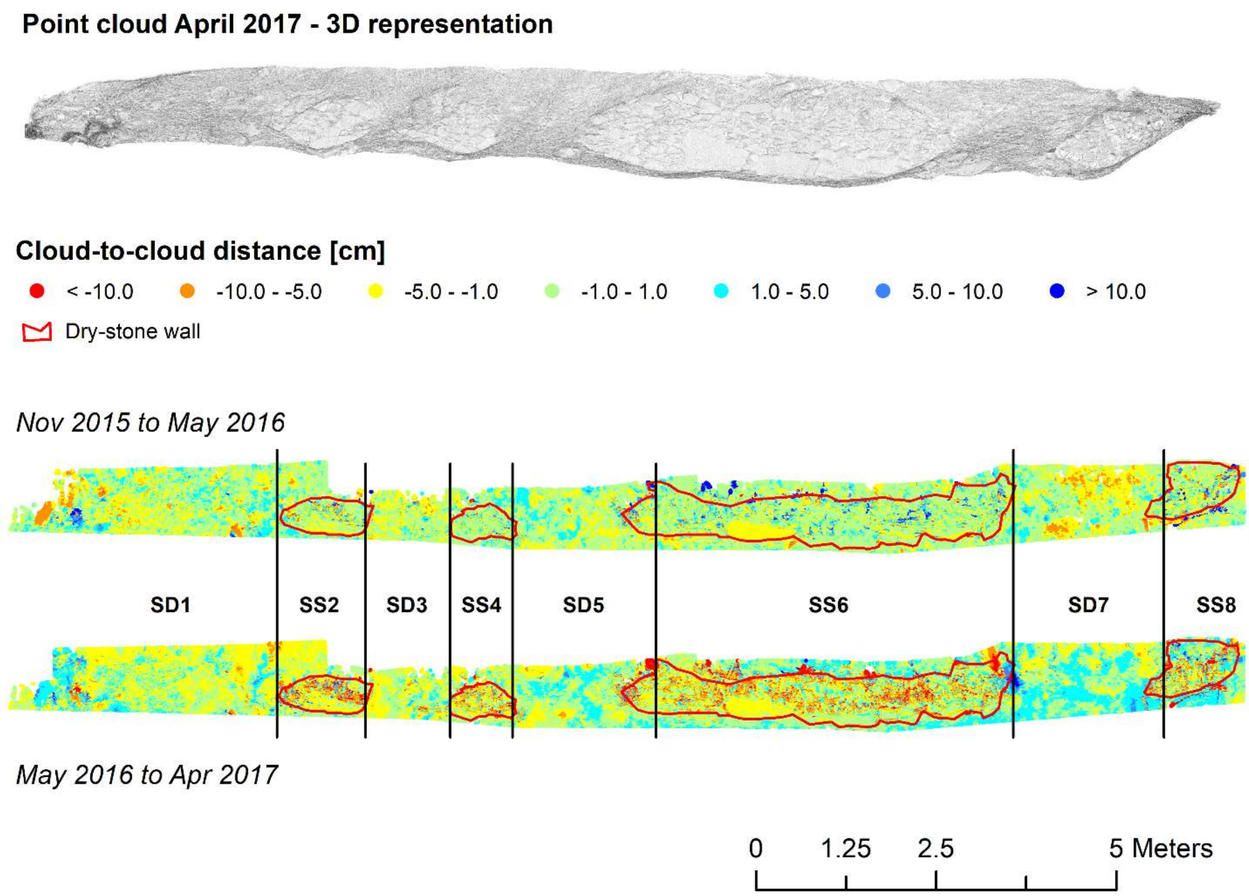

Fig. 7: 3D representation of the point cloud acquired in April 2017 and cloud-to-cloud absolute distances (x-y-z) of the facade of the dry-stone wall for the periods November 2015 – May 2016 and May 2016 – April 2017. SD indicate degraded sections, SS are standing sections. Dry-stone wall polygons represent standing sections of wall.

Negative changes over the entire survey period (end of November 2015 – beginning of April 2017) account for 179.2 kg, and include soil, stones and vegetation losses. The uncertainty interval of this value ranges between 174.2 and 185.1 kg and is related to instrument accuracy. The positive changes amount to 121.0 kg (range 114.5 – 123.6 kg), thus resulting in a net soil loss (negative minus positive) of 58.1 kg (50.7 –70.6 kg) in the scanned area. The two time periods between scans show a similar behavior; in the first six months a net soil loss of 22.6 kg is observed, while in the following 11 months a net soil loss of 35.5 kg is recorded. Also, it can be noticed that the error introduced by the unfiltered vegetation is lower than the uncertainty related to the instrument accuracy.

Table 3: Summary of the laser scanner surveys. SD means degraded section, SS means standing section. Season 1 is November 2015 - May 2016, Season 2 is May 2016 - April 2017. In parenthesis, the uncertainty range due to instrument accuracy.

Section	Length [m]	Soil loss Season 1 [Mg ha^{-1}]	Soil loss Season 2 [Mg ha^{-1}]	Soil gain Season 1 [Mg ha^{-1}]	Soil gain Season 2 [Mg ha^{-1}]
SD1	3.6	4.1 (3.9 – 4.2)	3.0 (2.9 – 3.1)	1.9 (1.9 – 2.0)	1.7 (1.6 – 1.7)
SD3	1.3	1.8 (1.8 – 1.9)	2.4 (2.4 – 2.5)	1.2 (1.2 – 1.3)	0.8 (0.7 – 0.8)
SD5	1.8	2.0 (1.9 – 2.2)	2.5 (2.5 – 2.6)	2.9 (2.8 – 3.0)	1.5 (1.4 – 1.5)
SD7	2.2	4.7 (4.6 – 4.8)	1.3 (1.3 – 1.4)	1.4 (1.3 – 1.5)	3.7 (3.6 – 3.8)
SS2	1.3	1.0 .0.9 – 1.0)	2.0 (2.0 – 2.1)	1.1 (1.0 – 1.2)	0.4 (0.4 – 0.4)
SS4	0.8	0.6 (0.6 – 0.6)	0.8 (0.8 – 0.8)	0.9 (0.8 – 0.9)	0.3 (0.3 – 0.3)
SS6	5.0	1.1 (1.1 – 1.2)	1.7 (1.7 – 1.7)	1.0 (0.9 – 1.0)	0.8 (0.8 – 0.8)
SS8	1.1	1.0 (1.0 – 1.0)	1.6 (1.5 – 1.6)	1.8 (1.8 – 1.8)	1.2 (1.1 – 1.2)

Degraded sections lost, on average, 3.1 Mg ha^{-1} soil during Season 1 and 2.3 Mg ha^{-1} during Season 2, while for the same periods standing sections lost 0.9 Mg ha^{-1}and 1.5 Mg ha^{-1}, respectively. Therefore, over the entire period, the ratio between soil loss at degraded and standing sections of dry-stone wall for the scanned area is equal to 2.2, which is a lower ratio value to that calculated from traps (3.8). Yet, this value is not directly comparable to that calculated from traps. Scans do not capture the continuity of the soil erosion process but give a snapshot in time, thus partly explaining it. With TLS, the losses on which the erosion rates were calculated represent a minimum value of mobilized sediment. In fact, losses might be partially or completely filled during consecutive events, while gains might be partially or completely removed. These changes are not shown by 3D models performed periodically, considering that several erosion events can occur between survey periods.

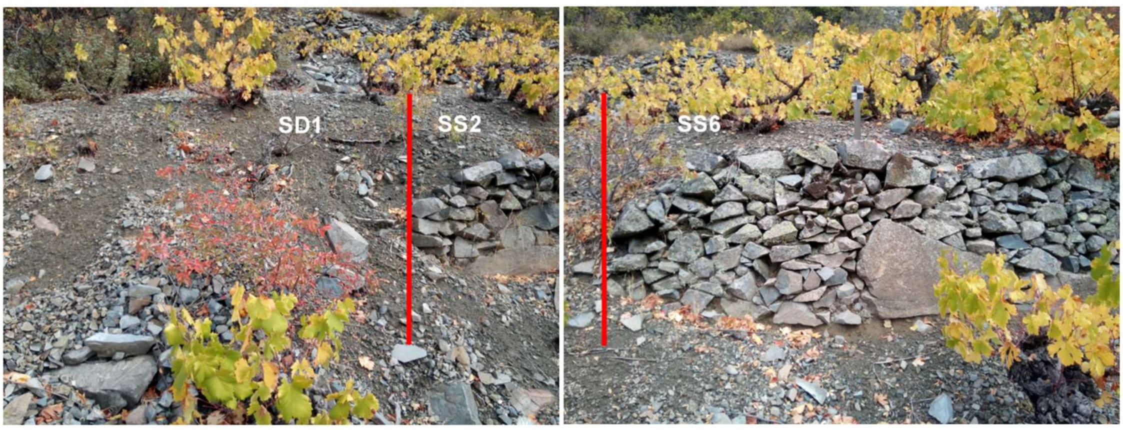

Fig. 8: Images of sections SD1 and a small part of SS2 (left), and section SS6 (right).

5 Discussion

5.1 Effectiveness of agricultural terraces in reducing soil erosion rates

Dorren and Rey (2004) reviewed the effects of terraces on erosion stressing their role in quantitative terms. In particular, they report measured values of mean annual soil erosion in terraced hillslopes and comparable non-terraced environments, with the effectiveness ranging from 50% in the sub-tropical Paranà (Brazil) to more than 95% in Malaysia. In a more recent review, Tarolli et al. (2014) focused mainly on the processes responsible for land degradation in abandoned terraced environments but without quantifying the differences between preserved and degrading structures. In a soil erosion study conducted in Ethiopia, Desta et al. (2005) found that plot terracing with stone bunds reduced soil water erosion by 68%. Based on literature data from 14 plots, Maetens et al. (2012) found that terraces were reducing erosion by an average factor of 0.75, compared to controlled plots without terraces. This factor lies within the range reported by Dorren and Ray (2004). Nunes et al. (2016) found very low soil erosion rates (0.015 Mg ha^{-1} y^{-1}) on a terraced field grown with pasture in Portugal. Bevan and Connelly (2011) applied a RUSLE3D soil erosion model in Antikythera (Greece), to quantify the mean soil erosion rates in terraced and non-terraced environments; the latter can be considered an indication of fully degraded terraced environment. They found that terraces decrease mean soil erosion rates by 56% (2.3 Mg ha^{-1} y^{-1}), compared to areas without terraces (5.2 Mg ha^{-1} y^{-1}). Djuma et al. (2017) modelled soil erosion processes along slope profiles in Cyprus with PESERA and found that hillslopes with well-maintained terraces produce erosion rates 10 times lower (0.15 Mg ha^{-1} y^{-1} with a 3% gradient) than the same hillslope without terraces (1.6 Mg ha^{-1} y^{-1} with a 47% gradient). In this case the calculated reduction of soil erosion rates due to terracing is around 91%.

The effectiveness of terraces in Cyprus, as indicated by the soil erosion reduction factor of 0.73 from the field experiment in the present study, concurs with the average results of Maetens et al. (2012), with the measured values of Desta et al. (2005), and lies within the range reported by Dorren and Rey (2004). Also, in terms of annual soil erosion rates, the results of this study are comparable (same order of magnitude) to those modelled by Bevan and Connelly (2011) and Djuma et al. (2017), in very similar environments. Although our results coincide with previous studies, it is necessary to stress that this study does not compare terraced and non-terraced hillslopes. Rather it focuses on a single degrading hillslope, where terraces are collapsing and an equilibrium, in terms of slope gradient, has not been reached yet. In terms of soil erosion rates over wider terraced environments, Lesschen et al. (2008) report an average value of 87 Mg ha^{-1} y^{-1} for a small abandoned watershed in Spain (30 km^2). This value is much higher than the 2.4-3.2 Mg ha^{-1} y^{-1} range measured in this study. However, the authors surveyed the watershed by differential GPS 22 years after abandonment, and their assumption that the terraces were in perfect state prior to abandonment, could have overestimated the erosion rates.

5.2 Soil erosion rates in vineyards

Focusing on vineyards, Rodrigo-Comino (2018) reported a variability of soil erosion rates measured by erosion plots in different areas of the world (including Europe, western US, Chile, and southern Australia) that spans from below 1 Mg ha^{-1} y^{-1} to around 75 Mg ha^{-1} y^{-1}. From the boxplots presented in his study, the median value is around 8 Mg ha^{-1} y^{-1}, the average is around 19 Mg ha^{-1} y^{-1}, while the inter-quantile range extends from 2 to 25 Mg ha^{-1} y^{-1}. In the study, there is no specific reference to agricultural terraces. In the Mediterranean region, Prosdocimi et al. (2016) reported that erosion plots are the most common method applied for the measurement of soil erosion rates in vineyards. They found soil erosion rates from erosion plots between 0.02 and 41.50 Mg ha^{-1} y^{-1} in the literature. Similar to Rodrigo-Comino (2018), no specific reference to soil erosion rates on agricultural terraces is presented by Prosdocimi et al. (2016). Panagos et al. (2015a) presented a European wide soil erosion assessment based on RUSLE. They included support practices - i.e., contour farming, stone walls, and grass margins - in their calculations though the use of the factor *P* (Panagos et al., 2015b) and for the research area of this paper they reported a soil erosion rate around 7 Mg ha^{-1} y^{-1}. This value is more than double the erosion rate derived in this study, but it is within the same order of magnitude. Also, our results present a mid-order of magnitude compared to the ranges presented by both Rodrigo-Comino (2018) and Prosdocimi et al. (2016). Hence, for vineyards, the range of soil erosion rates observed at our monitoring site can be considered medium-low but not negligible, being also larger than the upper limit of the European tolerable rate of 1.4 Mg ha^{-1} y^{-1} (Verheijen et al., 2009). It should be noted that at standing sections of dry-stone wall, the measured erosion rates for the two monitoring seasons (1.0 and 0.9 Mg ha^{-1} y^{-1}, respectively) are tolerable, according to this European standard (Table 1). Maintaining agricultural terraces could therefore be an effective measure to contain soil erosion rates within tolerable limits.

5.3 Degradation factors in terraced environments

The detailed topographic survey enabled the linkage of traps to the derived drainage areas upslope from the monitored wall sections. It was found that two or more consecutive degraded walls along the flow accumulation path of a single trap could increase soil erosion rates, which are strictly related to both rainfall intensities (for particle detachment) and runoff (for transport), as suggested by Nearing et al. (2017), and testified by the high correlation with the runoff ratio erosivity index. This finding is in line with the study of Meerkerk et al. (2009) conducted in a 475-ha watershed in Spain. These authors found that collapsing terraces resulted in a significant increase in connectivity and discharge. It was also noted that standing and degraded sections of the dry-stone wall had similar-sized upslope drainage areas, indicating that wall failures could have been caused by other processes than surface runoff and erosion. Preti et al. (2017) suggested a predominant role of rapid infiltration and fast, concentrated subsurface flow in discontinuities or preferential flow paths. Camera et al. (2014b, 2015) also stress the important role that subsurface flow - and the factors that influence it – is inducing dry-stone wall collapse. Weaknesses in the dry-stone wall structure caused by poor construction could be another possible cause of collapse (Liniger et al., 2008; Zoumides, 2015). In general, Table 2 values need to be interpreted with caution; obstructions finer than the raster cells (e.g. stones) and features not included in the topography (e.g. plants) can change the expected flow accumulation paths of surface runoff. Also, small stones could move between two consecutive erosion events, potentially affecting flow concentration paths, but the DEM could not be modified accordingly. These potential changes are partly addressed by considering the minimum and maximum trap area ranges, but larger differences could occur.

5.4 Range-based techniques for land degradation assessment

Many authors have reported the reliability of ground-based laser scanner for fast acquisition of high-resolution and high-precision surface elevation data, i.e. the capacity of TLS to support micro-topography studies and the investigation of related processes (Westoby et al., 2012). Successful applications span from the study of grain-scale morphology of fluvial sediments and its effects on erosional-depositional riverine dynamics (e.g., Hodge et al., 2009), to the investigation of surface roughness effects on concentrated flow erosion (e.g., Eitel et al., 2011), and the multi-temporal analysis of micro-topography changes to investigate overland, rill and gully erosion processes (e.g., DeLong et al., 2018; Kociuba et al., 2015). Also, Preti et al. (2013) applied TLS to derive a high-resolution model (0.01 m) of a dry-stone wall that allowed the recognition of single wall stones. The authors scanned a 120-m long wall, from five scanning positions, to obtain a model to be used for stress-strain analyses. Unlike our study, where TLS multi-temporal analysis was applied to evaluate the degradation of dry-stone walls, they did not perform any degradation analysis based on multi-temporal scans. However, our approach showed some limitations due to irregular reflections from the voids between the stones, resulting in fictitious displacements. The multi-temporal scans were georeferenced through targets placed on the ground before the first acquisition, but scanning positions, selected to reduce the obstruction of the vegetation cover, varied for the three surveys. Different scanning angles could be the cause of the irregular reflections. However, the multi-temporal TLS surveys provided useful information for the study of soil erosion in terraced environments, in terms of differentiation between soil losses and soil gains. Given the potential of the method, as suggested by the numerous successful applications and some outcomes of this study, further research could focus on the development of a more rigorous acquisition and post-processing procedure for multi-temporal analysis of dry-stone wall degradation.

Another limitation of TLS surveys is the broad temporal resolution of the monitoring in comparison to continuous monitoring with sediment traps (data after every rainfall event). As they are presented and applied in this study, the two methods cannot be compared, but they are complementary to each other. Recently, Eltner et al. (2017) studied erosion during a single rainfall event using a photogrammetric time-lapse method. Images were acquired every 15 seconds and a system for automatic data acquisition and processing was established. Photogrammetry should be tested for multi-temporal analysis of dry-stone wall degradation as well, since the effects of traditional problems related to the technique – such as shadows, vegetation, camera calibration and boundary distortion (Eltner et al., 2016) – require further investigation. This approach could potentially bridge the temporal resolution gap between traps and 3D models, so that comparison of the results of the two methods, which is currently lacking in the literature, could be carried out.

6 Conclusions

The main conclusions of this study are summarized below:

- Soil erosion from a terraced field cultivated with grapevines, with 50% average slope and 31.5-m length, monitored during a two-year period was 2.4 Mg ha^{-1} y^{-1}, assuming a linear slope. This value could be as high as 3.2 Mg ha^{-1} y^{-1}, based on the contributing drainage area, derived from a high-resolution topographic survey.
- Soil erosion monitored at standing and degraded sections of the dry-stone wall indicated that terrace maintenance could reduce soil erosion by a factor of 3.8. This would reduce the soil erosion of the studied terraced field to 1.0 Mg ha^{-1} y^{-1}.
- Maximum 10- and 30-minute rainfall intensity explained a larger portion of the variance of the measured soil erosion than the 60-minute rainfall intensity, although differences are minor.
- Soil erosion rates were affected by the interception of consecutive degraded sections of dry-stone wall along upslope flow accumulation paths. However, dry-stone wall failure could not be linked exclusively to hydrologic processes.
- Laser scanner data could add information about soil erosion processes at degraded sections of wall, identifying the soil scarp eroding back after the collapse of the stones and areas characterized by soil losses and soil gains.
- The presented multi-temporal laser scanner survey approach could not furnish reliable information on dry-stone wall degradation processes because of artifacts in the data created by the voids between the irregularly shaped and arranged stones. Further research should focus on developing a more rigorous acquisition and post-processing procedure.

Overall, the experimental design proved to be effective for quantifying the amount of soil eroded in a typical terraced vineyard, for comparing erosion rates from standing and degraded dry-stone walls, and for analyzing relations between erosion and rainfall intensities and erosivities. However, the studied human-modified natural environment is extremely variable, therefore to represent this variability and allow more robust conclusions more traps are needed on the same terrace. Further research on the application and optimization of range-based and imaging techniques to link soil erosion and dry-stone wall degradation processes is also needed.

Acknowledgements

We would like to thank the Alona community council members for their cooperation, as well as Mr. Andreas Tsiakkas and Mr. Kleopas Stylianou for allowing us to do the monitoring research in their fields. We would also like to thank Aitor Herrero, Nancy al Haddad and Sarah Tlais for their help with the soil sieving and weighting. We are grateful to the Cyprus Department of Meteorology and the Cyprus Agricultural Payment Organization for providing data. We also thank the three anonymous reviewers and the guest editor, who helped to improve the quality of this manuscript. This research has received funding from the European Union Seventh Framework Programme (FP7/2007–2013) under grant agreement no. 603498 (RECARE project).

References

Arnáez, J., Lasanta, T., Errea, M.P., Ortigosa, L., 2011. Land abandonment, landscape evolution, and soil erosion in a Spanish Mediterranean mountain region: the case of Camero Viejo. Land Degrad. Develop. 22, 537–550. doi: 10.1002/ldr.1032.

Balaguer-Puig, M., Marques-Mateu, A., Lerma, J.L., Ibanez-Asensio, S., 2017. Estimation of small-scale soil erosion in laboratory experiments with Structure from Motion photogrammetry. Geomorphology 295, 285-296. doi: 10.1016/j.geomorph.2017.04.035.

Bevan, A., Conolly, J., 2011. Terraced fields and Mediterranean landscape structure: An analytical case study from Antikythera, Greece. Ecological Modelling 222, 1303-1314. doi: 10.1016/j.ecolmodel.2010.12.016.

Biddoccu, M., Ferraris, S., Pitacco, A., Cavallo, E., 2017. Temporal variability of soil management effects on soil hydrological properties, runoff and erosion at the field scale in a hillslope vineyard, North-West Italy. Soil & Tillage Research 165, 46-58. doi: 10.1016/j.still.2016.07.017.

Bracken, L., Kirkby, M., 2005. Differences in hillslope runoff and sediment transport rates within two semi-arid catchments in southeast Spain. Geomorphology 68, 183–200. doi: 10.1016/j.geomorph.2004.11.013

Brandolini, P., Cevasco, A., Capolongo, D., Pepe, G., Lovergine, F., Del Monte, M., 2017. Response of terraced slopes to a very intense rainfall event and relationships with land abandonment: A Case study from Cinque Terre (Italy). Land Degrad. Develop. doi: 10.1002/ldr.2672.

BS ISO 11277, 2009. Soil quality - Determination of particle size distribution in mineral soil material - Method by sieving and sedimentation.

Camera C., Apuani, T., Masetti, M., 2014b. Mechanisms of failure on terraced slopes: the Valtellina case (northern Italy). Landslides 11, 43-54. doi: 10.1007/s10346-012-0371-3.

Camera C., Apuani, T., Masetti, M., 2015. Modelling the stability of terraced slopes: an approach from Valtellina (Northern Italy). Env. Earth Sci. 74, 855-868. doi: 10.1007/s12665-015-4089-0.

Camera, C., Bruggeman, A., Hadjinicolaou, P., Pashiardis, S., Lange, M.A., 2014a. Evaluation of interpolation techniques for the creation of gridded daily precipitation (1 × 1 km2); Cyprus, 1980–2010. J. Geophys. Res. Atmos. 119, 693-712. doi: 10.1002/2013JD020611.

Cerdà, A., 1997. Soil erosion after land abandonment in a semiarid environment of Southeastern Spain. Arid Soil Research and Rehabilitation 11, 163-176.

Cerdà, A., Keesstra, S.D., Rodrigo-Comino, J., Novara, A., Pereira, P., Brevik, E., Giménez-Morera, A., Fernández-Raga, M., Pulido, M., di Prima, S., Jordán, A., 2017. Runoff initiation, soil detachment and connectivity are enhanced as a consequence of vineyards plantations. Journal of Environmental Management 202, 268-275. doi: 10.1016/j.jenvman.2017.07.036.

Chow, T.L., Rees, H.W., and Daigle, J.L., 1999. Effectiveness of terraces grassed waterway systems for soil and water conservation: a field evaluation. Journal of Soil and Water Conservation 54, 577-583.

DeLong, S.B., Youberg, A.M., DeLong, W.M., Murphy, B.P., 2018. Post-wildfire landscape change and erosional processes from repeat terrestrial lidar in a steep headwater catchment, Chiricahua Mountains, Arizona, USA. Geomorphology 300, 13-30. doi: 10.1016/j.geomorph.2017.09.028.

Desta, G., Nyssen, J., Poesen, J., Deckers, J., Mitiku, H., Govers, G., Moeyersons, J., 2005. Effectiveness of stone bunds in controlling soil erosion on cropland in the Tigray highlands, Northern Ethiopia. Soil Use Manage. 21, 287–297. doi: lO.l079/SUM2005321.

Di Stefano, C., Ferro, V., Palmeri, V., Pampalone, V., 2017. Measuring rill erosion using structure from motion: A plot experiment. Catena 156, 383-392. doi: 10.1016/j.catena.2017.04.023.

Djuma, H., Bruggeman, A., Camera, C., Zoumides, C., 2017. Combining qualitative and quantitative methods for soil erosion assessments: an application in a sloping Mediterranean watershed, Cyprus. Land Degrad. Dev. 28, 243-254. doi: 10.1002/ldr.2571.

Dorren, L., Rey, F., 2004. review of the effect of terracing on erosion. In: van Asselen, S., Boix-Fayons, C., Imeson, A. (Eds.), Briefing papers of the 2nd SCAPE Workshop, Cinque Terre, Italy, 97-108.

Eitel, J.U.H., Williams, C.J., Vierling, L.A., Al-Hamdan, O.Z., Pierson, F.B., 2011. Suitability of terrestrial laser scanning for studying surface roughness effects on concentrated flow erosion processes in rangelands. Catena 87, 398-407. doi: 10.1016/j.catena.2011.07.009.

Eltner, A., Baumgart, P., 2015. Accuracy constraints of terrestrial Lidar data for soil erosion measurement: Application to a Mediterranean field plot. Geomorphology 245, 243–254. doi: 10.1016/j.geomorph.2015.06.008.

Eltner, A., Kaiser, A., Castillo, C., Rock, G., Neugirg, F., Abellán, A., 2016. Image-based surface reconstruction in geomorphometry – merits, limits and developments. Earth Surf. Dynam. 4, 359–389. doi: 0.5194/esurf-4-359-2016.

Eltner, A., Kaiser, A., Abellán, A., Schindewolf, M., 2017. Time lapse structure-from-motion photogrammetry for continuous geomorphic monitoring. Earth Surf. Process. Landforms 42, 2240-2253. doi: 10.1002/esp.4178.

Fall, P.L., Falconer, S.E., Galletti, C.S., Shirmang, T., Ridder, E., Klinge J., 2012. Long-term agrarian landscapes in the Troodos foothills, Cyprus. J. Archaeol. Sci. 39, 2335-2347. doi: 10.1016/j.jas.2012.02.010.

Frankl, A., Stal, C., Abraha, A., Nyssen, J., Rieke-Zapp, D., DeWulf, A., Poesen, J., 2015. Detailed recording of gully morphology in 3D through image-based modelling. Catena 127, 92-101. doi: 10.1016/j.catena.2014.12.016.

García-Ruiz, J.M., Lana-Renault, N., 2011. Hydrological and erosive consequences of farmland abandonment in Europe, with special reference to the Mediterranean region–a review. Agriculture, Ecosystems & Environment 140, 317–338. DOI: 10.1016/j.agee.2011.01.003.

Gexcel, 2017. JRC 3D Reconstructor Software Manual. Gexcel, Brescia (Italy), 196 pp. Available at: http://www.gexcel.homeip.net/Reconstructor/R_Manual/2017_R_Manual_EN.pdf [Last Accessed: 15/12/2017]

Gomez-Gutierrez, A., Schnabel, S., Berenguer-Sempere, F., Lavado-Contador, F., Rubio-Delgado, J., 2014. Using 3D photo-reconstruction methods to estimate gully headcut erosion. Catena 120, 91-101. doi: 10.1016/j.catena.2014.04.004.

Hodge, R., Brasington, J., Richards, K., 2009. In-situ characterisation of grain-scale fluvial morphology using Terrestrial Laser Scanning. Earth Surf. Process. Landforms 34, 954-968. doi:10.1002/esp.1780.

Hoogsteen, M.J.J., Lantinga, E.A., Bakker, E.J., Groot, J.C.J., Tittonell, P. A., 2015. Estimating Soil Organic Carbon through Loss on Ignition: Effects of Ignition Conditions and Structural Water Loss. European Journal of Soil Science 66, 320–28. doi:10.1111/ejss.12224.

Inbar, M., Llerena, C.A., 2000. Erosion processes in high mountain agricultural Terraces in Peru` Mt. Res. Dev. 20, 72–79. Doi: 10.1659/0276-4741(2000)020[0072:EPIHMA]2.0.CO;2

Kinnell, P.I.A., 2014. Applying the Q_REI30 index within the USLE modelling environment. Hydrol. Process. 28, 591–598. doi:10.1002/hyp.9591.

Kirkby, M.J., Irvine, B.J., Jones, R.J.A., Govers, G., Boer, M., Cerdan, O., Daroussin, J., Gobin, A., Grimm, M., Le Bissonnais, Y., Kosmas, C., Mantel, S., Puigdefabregas, J., Van Lynden, G., 2008. The PESERA coarse scale erosion model for Europe. I. Model rationale and implementation. European Journal of Soil Sciences 59, 1293–306. doi:10.1111/j.1365-2389.2008.01072.x.

Kociuba, W., Janicki, G., Rodzik, J.,; Stepniewski, K., 2015. Comparison of volumetric and remote sensing methods (TLS) for assessing the development of a permanent forested loess gully. Nat. Hazards 79, S139-S158. doi: 10.1007/s11069-015-1807-6.

Koulouri, M., Giourga, C., 2007. Land abandonment and slope gradient as key factors of soil erosion in Mediterranean terraced lands. Catena 69, 274-281.

Lesschen, J.P., Cammeraat, L.H., Nieman, T., 2008. Erosion and terrace failure due to agricultural land abandonment in a semi-arid environment. Earth Surf. Process. Landforms 33, 1574-1584. doi: 10.1002/esp.1676.

Li, X.H., Yang, J., Zhao, C.Y., Wang, B., 2014. Runoff and sediment from orchard terraces in southeastern China. Land Degradation & Development 25, 184-192. doi:10.1002/ldr.1160.

Lieskovsky, J., Kenderessy, P., 2014. Modelling the effect of vegetation cover and different tillage practices on soil erosion in vineyards: a case study in Vràble (Slovakia) using WATEM/SEDEM. Land Degrad. Develop. 25, 288–296. doi: 10.1002/ldr.2162.

Liniger H, Schwilch G, Gurtner M, Mekdaschi SR, Hauert C, van Lynden G, Critchley W. 2008. A Framework for Documentation and Evaluation of Sustainable Land Management – Technologies Basic WOCAT Questionnaire. WOCAT-CDE: Bern

Maetens, W., Poesen, J., Vanmaercke M., 2012. How effective are soil conservation techniques in reducing plot runoff and soil loss in Europe and the Mediterranean? Earth Sci. Rev. 115, 21–31.

Mangiafico, S.S., 2016. Summary and Analysis of Extension Program Evaluation in R, version 1.10.0. rcompanion.org/handbook/.

Meerkerk, A.L., van Wesemael, B., Bellin, N., 2009. Application of connectivity theory to model the impact of terrace failure on runoff in semi-arid catchments. Hydrol. Process. 23, 2792–2803. doi: 10.1002/hyp.7376.

Modica, G, Praticò, S., Di Fazio, S., 2017. Abandonment of traditional terraced landscape: A change detection approach (a case study in Costa Viola, Calabria, Italy). Land Degrad. Develop. 28, 2608–2622. doi: 10.1002/ldr.2824

Napoli, M., Dalla Marta, A., Zanchi, C.A., Orlandini, S., 2017. Assessment of soil and nutrient losses by runoff under different soil management practices in an Italian hilly vineyard. Soil & Tillage Research 168, 71-80. doi: 10.1016/j.still.2016.12.011.

Nasta, P., Palladino, M., Ursino, N., Saracino, A., Sommella, A., Romano, N., 2017. Assessing long-term impact of land-use change on hydrological ecosystem functions in a Mediterranean upland agro-forestry catchment. Sci. Tot. Environ. 605, 1070-1082. doi: 10.1016/j.scitotenv.2017.06.008.

Nearing, M.A., Yin, S., Borrelli, P., Polyakov, V.O., 2017. Rainfall erosivity: An historical review. Catena 157, 357–362. doi: 10.1016/j.catena.2017.06.004.

Nouwakpo, S.K., Weltz, M.A., McGwire, K., 2016. Assessing the performance of structure-from-motion photogrammetry and terrestrial LiDAR for reconstructing soil surface microtopography of naturally vegetated plots. Earth Surf. Process. Landforms 41, 308–322. doi: 10.1002/esp.3787.

Nunes, J.P, Bernard-Jannin, L., Rodríguez Blanco, M.L., Santos, J.M., Coelho, C.O.A., Keizer, J.J., 2016. Hydrological and erosion processes in terraced fields: observations from a humid Mediterranean region in northern Portugal. Land Degradation and Development. doi: 10.1002/ldr.2550

Orem, C., Pelletier, J., 2015. Quantifying the time scale of elevated geomorphic response following wildfires using multi-temporal LiDAR data: an example from the Las Conchas fire, Jemez Mountains, New Mexico. Geomorphology 232, 224–238. doi: 10.1016/j.geomorph.2015.01.006.

Panagos, P., Borrelli, P., Poesen, J., Ballabio, C., Lugato, E., Meusburger, K., Montanarella, L., Alewell, C., 2015a. The new assessment of soil loss by water erosion in Europe. Environ. Sci. Policy 54, 438-447. doi.org/10.1016/j.envsci.2015.08.012.

Panagos, P., Borrelli, P., Meusburger, K., van der Zanden, E.H., Poesen, J., Alewell, C., 2015b. Modelling the effect of support practices (P-factor) on the reduction of soil erosion by water at European scale. Environmental Science & Policy 51, 23–34. doi: 10.1016/j.envsci.2015.03.012.

Preti, F., Guastini, E., Penna, D., Dani, A., Cassiani, G., Boaga, J., Deiana, R., Romano, N., Nasta, P., Palladino, M., Errico, A., Giambastiani, Y., Trucchi, P., and Tarolli, P., 2018. Conceptualization of water flow pathways in agricultural terraced landscapes. Land Degrad. Develop., 29, 651–662. doi: 10.1002/ldr.2764.

Preti, F., Tarolli, P., Dani, A., Calligaro, S., Prosdocimi, M., 2013. LiDAR derived high resolution topography: the next challenge for the analysis of terraces stability and vineyard soil erosion. Journal of Agricultural Engineering 44, 85-89. doi: 10.4081/jae.2013.258.

Prosdocimi, M., Calligaro, S., Sofia, G., Dalla Fontana, G., Tarolli, P., 2015. Bank erosion in agricultural drainage networks: new challenges from structure-from-motion photogrammetry for post-event analysis. Earth Surf. Process. Landforms 40, 1891–1906. doi: 10.1002/esp.3767.

Prosdocimi, M., Cerdà, A., Tarolli, P., 2016. Soil water erosion on Mediterranean vineyards: A review. Catena 141, 1-21. doi: 10.1016/j.catena.2016.02.010.

Renard, K.G., Foster, G.R., Weesies, G.A., McCool, D.K., Yoder, D.C., 1997. Predicting soil erosion by water: a guide to conservation planning with the Revised Universal Soil Loss Equation (RUSLE). In: USDA Agriculture Handbook. 703 D.C, Washington 404 pp.

Rodrigo Comino, J., 2018. Five decades of soil erosion research in "terroir". The state-of-the-art. Earth-Science Reviews 179, 436–447. doi: 10.1016/j.earscirev.2018.02.014.

Rodrigo Comino, J., Ruiz Sinoga, J.D., Senciales González, J.M., Guerra-Merchán, A., Seeger, M., Ries, J.B., 2016. High variability of soil erosion and hydrological processes in Mediterranean hillslope vineyards (Montes de Málaga, Spain). Catena 145, 274–284. doi: 10.1016/j.catena.2016.06.012.

Rolé, A., 2007. The terraced landscapes of the Maltese islands. In Europe's living landscapes, Essays exploring our identity in the countryside. Pedroli, G.B.M., van Doorn, A.M., De Blust, G., Wascher, D.M., Bunce, F. (Eds), KNNV publishing, Zeist, 405–420. doi: 10.1163/9789004278073_025.

Smith, M.W., Vericat D., 2015. From experimental plots to experimental landscapes: topography, erosion and deposition in sub-humid badlands from Structure-from-Motion photogrammetry. Earth Surface Processes and Landforms 40, 1656-1671. doi: 10.1002/esp.3747.

Staley, D., Wasklewicz, T., Kean, J., 2014. Characterizing the primary material sources and dominant erosional processes for post-fire debris-flow initiation in a headwater basin using multi-temporal terrestrial laser scanning data. Geomorphology 214, 324–338. doi: 10.1016/j.geomorph.2014.02.015.

Tarolli, P., Calligaro, S., Cazorzi, F., Dalla Fontana, G., 2013. Recognition of surface flow processes influenced by roads and trails in mountain areas using high-resolution topography. Eur. J. Remote Sens. 46, 176–197. doi: 10.5721/EuJRS20134610.

Tarolli, P., Preti, F., Romano, N., 2014. Terraced landscapes: from an old best practice to a potential hazard for soil degradation due to land abandonment. Anthropocene 6, 10 - 25. doi:10.1016/j.ancene.2014.03.002.

Tarolli, P., Sofia, G., Calligaro, S., Prosdocimi, M., Preti, F., Dalla Fontana, G., 2015. Vineyards in terraced landscapes: New opportunities from Lidar data. Land Degrad. Develop. 26, 92–102. doi: 10.1002/ldr.2311.

Topp, G.C., David, J.L., Annan, A.P., 1980. Electromagnetic Determination of Soil Water Content: Measurement in Coaxial Transmission Lines. Water Resources Research 16, 574-582. Doi: 10.1029/WR016i003p00574

Torquati, B., Giacchè, G., Venanzi, S., 2015. Economic analysis of the traditional cultural vineyard landscapes in Italy. Journal of Rural Studies 39, 122-132. doi:10.1016/j.jrurstud.2015.03.013.

USDA-Agricultural Research Service, 2013. Science Documentation Revised Universal Soil Loss Equation Version 2. Available at: https://www.ars.usda.gov/ARSUserFiles/60600505/RUSLE/RUSLE2_Science_Doc.pdf (last accessed 30/05/2018).

USDA Soil Survey Staff, 2014. Kellogg Soil Survey Laboratory Methods Manual. Soil Survey Investigations Report No. 42, Version 5.0. R Burt and Soil Survey Staff (ed.), U.S. Department of Agriculture, Natural Resources Conservation Service, 1031 pp.

Verheijen, F.G.A., Jones, R.J.A., Rickson, R.J., Smith, C.J., 2009. Tolerable versus actual soil erosion rates in Europe. Earth Sci. Rev. 94, 23–38. doi: 10.1016/j.earscirev.2009.02.003.

Westoby, M.J., Brasington, J., Glasser, N.F., Hambrey, M.J., Reynolds, J.M., 2012. 'Structure-from-Motion' photogrammetry: A low-cost, effective tool for geoscience applications. Geomorphology 179, 300-314. doi: 10.1016/j.geomorph.2012.08.021.

Widgren, M., 2007. Precolonial landesque capital: a global perspective. In: Hornborg, A., McNeill, J.R., Martinez-Alier, J., (Eds), Rethinking environmental history: world-system history and global environmental change, Altamira Press, Lanham, 61–77.

Wischmeier, W.H., Smith, D.D., 1958. Rainfall energy and its relation to soil loss. Trans. Am. Geophy. Union 39, 285–291.

Zittis, G., Bruggeman, A., Camera, C., Hadjinicolaou, P., Lelieveld, J., 2017. The added value of convection permitting simulations of extreme precipitation events over the eastern Mediterranean. Atmos. Res. 191, 20-33. doi: 10.1016/j.atmosres.2017.03.002.

Zoumides, C., 2015. Agricultural terraces with dry-stone walls – technologies 1702, Cyprus. WOCAT SLM Database. Available at: https://qcat.wocat.net/en/wocat/technologies/view/technologies_1702/ (last accessed 30/05/2018)

Zoumides, C., Bruggeman, A., Giannakis, E., Camera, C., Djuma, H., Eliades, M., Charalambous, K., 2017. Community-based rehabilitation of mountain terraces in Cyprus. Land Degrad. Dev. 28, 95-105. doi: 10.1002/ldr.2586.